Article

SUN proteins facilitate the removal of membranes from chromatin during nuclear envelope breakdown

TURGAY, Yagmur, *et al*.

Abstract

SUN proteins reside in the inner nuclear membrane and form complexes with KASH proteins of the outer nuclear membrane that connect the nuclear envelope (NE) to the cytoskeleton. These complexes have well-established functions in nuclear anchorage and migration in interphase, but little is known about their involvement in mitotic processes. Our analysis demonstrates that simultaneous depletion of human SUN1 and SUN2 delayed removal of membranes from chromatin during NE breakdown (NEBD) and impaired the formation of prophase NE invaginations (PNEIs), similar to microtubule depolymerization or down-regulation of the dynein cofactors NudE/EL. In addition, overexpression of dominant-negative SUN and KASH constructs reduced the occurrence of PNEI, indicating a requirement for functional SUN-KASH complexes in NE remodeling. Codepletion of SUN1/2 slowed cell proliferation and resulted in an accumulation of morphologically defective and disoriented mitotic spindles. Quantification of mitotic timing revealed a delay between NEBD and chromatin separation, indicating a role of SUN proteins in bipolar spindle assembly and mitotic [...]

Reference

TURGAY, Yagmur, *et al*. SUN proteins facilitate the removal of membranes from chromatin during nuclear envelope breakdown. *The Journal of Cell Biology*, 2014, vol. 204, no. 7, p. 1099-109

DOI : 10.1083/jcb.201310116
PMID : 24662567

Published March 24, 2014

SUN proteins facilitate the removal of membranes from chromatin during nuclear envelope breakdown

Yagmur Turgay,[1] Lysie Champion,[1] Csaba Balazs,[2] Michael Held,[1] Alberto Toso,[1] Daniel W. Gerlich,[1] Patrick Meraldi,[1] and Ulrike Kutay[1]

[1]Institute of Biochemistry, Department of Biology, and [2]Light Microscopy Center, Swiss Federal Institute of Technology Zurich, CH-8093 Zurich, Switzerland

SUN proteins reside in the inner nuclear membrane and form complexes with KASH proteins of the outer nuclear membrane that connect the nuclear envelope (NE) to the cytoskeleton. These complexes have well-established functions in nuclear anchorage and migration in interphase, but little is known about their involvement in mitotic processes. Our analysis demonstrates that simultaneous depletion of human SUN1 and SUN2 delayed removal of membranes from chromatin during NE breakdown (NEBD) and impaired the formation of prophase NE invaginations (PNEIs), similar to microtubule depolymerization or down-regulation of the dynein cofactors NudE/EL. In addition, overexpression of dominant-negative SUN and KASH constructs reduced the occurrence of PNEI, indicating a requirement for functional SUN–KASH complexes in NE remodeling. Codepletion of SUN1/2 slowed cell proliferation and resulted in an accumulation of morphologically defective and disoriented mitotic spindles. Quantification of mitotic timing revealed a delay between NEBD and chromatin separation, indicating a role of SUN proteins in bipolar spindle assembly and mitotic progression.

Introduction

When vertebrate cells enter mitosis, the nuclear envelope (NE) undergoes extensive structural changes in the process of NE breakdown (NEBD; Güttinger et al., 2009). During NEBD, NE membrane proteins are dissociated from nuclear binding partners and disperse into the ER, leading to the loss of NE identity.

NE disassembly is supported by a microtubule (MT)-dependent tearing process that promotes removal of membranes from chromatin (Beaudouin et al., 2002; Salina et al., 2002; Mühlhäusser and Kutay, 2007). In prophase, MT asters form around centrosomes and start moving apart along the NE. MT-dependent forces generated on astral MTs by NE-attached motors pull the NE membrane toward centrosomes, causing pocketlike membrane invaginations around centrosomes referred to as prophase NE invaginations (PNEIs). As a result of this tearing process, the NE fenestrates at one or several sites (Beaudouin et al., 2002; Salina et al., 2002; Rosenblatt, 2005; Mühlhäusser and Kutay, 2007).

MT-based NE remodeling in prophase and the subsequent clearance of NE/ER membranes from chromatin during prometaphase are dependent on the minus end–directed motor dynein (Beaudouin et al., 2002; Salina et al., 2002; Mühlhäusser and Kutay, 2007). So far, two pathways have been described that independently mediate dynein anchorage and centrosome tethering to the NE in early mitosis. Late in G2, the dynein adaptor BICD2 (Bicaudal D2) promotes dynein recruitment to the nucleoporin RanBP2/Nup358 (Splinter et al., 2010). Using a distinct mechanism, likely acting later during prophase, the dynein cofactor NudE/EL (nuclear distribution protein NudE homologue 1/nuclear distribution protein NudE–like 1) in complex with the kinetochore constituent CENP-F tethers dynein/dynactin to the scaffold nucleoporin Nup133 (Bolhy et al., 2011). NE-associated BICD2 and CENP-F support dynein-driven centrosome separation and bipolar spindle formation (Bolhy et al., 2011; Raaijmakers et al., 2012). It has, however, remained unclear which NE-dynein

Correspondence to Ulrike Kutay: ulrike.kutay@bc.biol.ethz.ch

Y. Turgay's present address is Dept. of Biochemistry, University of Zurich, CH-8057 Zurich, Switzerland.

D.W. Gerlich's present address is Institute of Molecular Biotechnology, 1030 Vienna, Austria.

P. Meraldi's present address is Centre Médical Universitaire, Université de Genève, CH-1211 Geneva, Switzerland.

Abbreviations used in this paper: DIC, dynein intermediate chain; DN, dominant negative; IBB, importin-β binding; INM, inner nuclear membrane; LBR, Lamin B receptor; LINC, linker of nucleoskeleton and cytoskeleton; MT, microtubule; NE, nuclear envelope; NEBD, NE breakdown; NPC, nuclear pore complex; ONM, outer nuclear membrane; PNEI, prophase NE invagination.

Supplemental Material can be found at:
http://jcb.rupress.org/content/suppl/2014/03/20/jcb.201310116.DC1.html
Original image data can be found at:
http://jcb-dataviewer.rupress.org/jcb/browse/7503

The Rockefeller University Press $30.00
J. Cell Biol. Vol. 204 No. 7 1099–1109
www.jcb.org/cgi/doi/10.1083/jcb.201310116

Published March 24, 2014

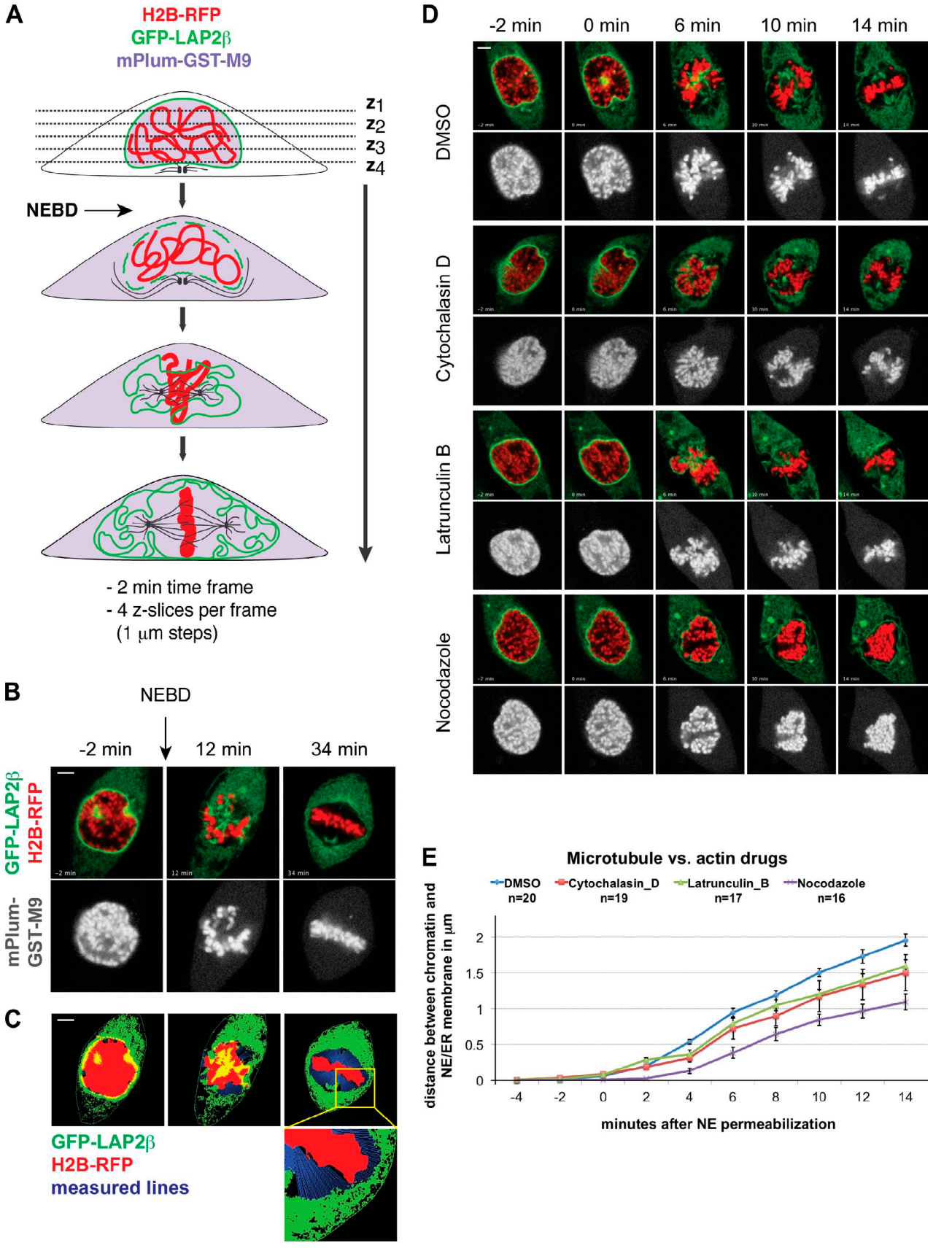

Figure 1. **Quantification of NE/ER membrane removal from chromatin.** (A) Experimental setup to monitor removal of NE/ER membranes from chromatin. HeLa cells stably expressing the INM protein GFP-LAP2β as an NE/ER marker, H2B-mRFP as a chromatin marker, and mPlum-GST-M9 as a nuclear efflux marker defining the onset of NEBD (t = 0 min) were used for live-cell confocal microscopy. Image acquisition of early prophase cells was performed every 2 min in four z slices. (B) Representative images of reporter cells before and after NEBD. Note that the strong emission of H2B-mRFP is also visible in the mPlum

Published March 24, 2014

tethering mechanism, if any, assists NE/ER membrane removal from chromatin.

Dynein-dependent clearance of the NE/ER network from chromatin continues during prometaphase, when disassembly of nuclear pore complexes (NPCs) has far advanced (Beaudouin et al., 2002; Salina et al., 2002; Mühlhäusser and Kutay, 2007). Thus, additional nucleoporin-independent pathways might contribute to MT-dependent NE/ER membrane remodeling at time points when NPCs have been largely disintegrated. Interestingly, the MT-binding ER proteins REEP3/4 have recently been shown to support clearance of ER membranes from chromatin in metaphase (Schlaitz et al., 2013).

Among other candidates for a function in MT-dependent NE/ER membrane remodeling are linker of nucleoskeleton and cytoskeleton (LINC) complexes, which support diverse processes involving motor-dependent force transmission across the NE (Crisp et al., 2006; Worman and Gundersen, 2006; Starr and Fridolfsson, 2010). LINC complexes form NE bridges composed of SUN (Sad1p and UNC-84 homology) and KASH (Klarsicht/Anc-1/SYNE homology) family members, which are integral membrane proteins of the inner nuclear membrane (INM) and outer nuclear membrane (ONM), respectively (Malone et al., 1999; Starr and Han, 2002). SUN and KASH proteins tightly interact with each other in the perinuclear space by binding of the luminal, C-terminal tails of KASH proteins to the conserved C-terminal domains of SUN proteins (Malone et al., 1999; Sosa et al., 2012). The N-terminal domains of KASH proteins protrude from the NE into the cytosol and interact with cytoskeletal structures, including actin filaments, intermediate filaments, and MT motors (Starr and Fridolfsson, 2010). Association of LINC complexes with dynein has been implicated in nuclear migration in worms (Malone et al., 1999; Fridolfsson et al., 2010) and mice (Zhang et al., 2009; Yu et al., 2011), in zygotic pronuclear congression (Malone et al., 2003), and meiotic movement of chromosomes along the NE from yeast to vertebrates (Chikashige et al., 2006; Morimoto et al., 2012; Wynne et al., 2012).

Here, we have explored the function of SUN proteins in mitosis. Our data demonstrate that SUN1 and SUN2 promote clearance of NE/ER membranes from chromatin during early prometaphase. Furthermore, depletion of SUN1/2 affects spindle assembly and cell cycle progression.

Results and discussion

Quantification of NE/ER membrane removal from chromatin

To analyze the removal of NE/ER membranes from chromatin during NEBD, we performed live-cell confocal microscopy using a HeLa cell line stably expressing the INM protein LAP2β-GFP as a NE/ER membrane marker, H2B-mRFP as a chromatin marker, and mPlum-GST-M9 as a nuclear efflux marker to define the starting point (0 min) of NEBD (Fig. 1). The distance between the innermost NE/ER membrane and the outermost chromatin signal was quantified along the lines of a radial grid over time.

To investigate the involvement of cytoskeletal components on NE/ER membrane removal, we added cytochalasin D, latrunculin B, or nocodazole to early prophase cells to depolymerize actin filaments or MTs (Fig. 1, D and E). Inhibition of actin polymerization did not affect initiation of ER/NE membrane removal but slowed down its progression to some extent. Inhibition of MT polymerization, however, delayed membrane clearance from chromatin, confirming earlier observations (Mühlhäusser and Kutay, 2007) and proving reliability of our automated quantification. Combined application of latrunculin B and nocodazole did not enhance the effect of nocodazole alone (unpublished data).

SUN1/2 codepletion delays NE/ER membrane removal

To assess the potential role of SUN proteins in NE/ER membrane removal, we depleted either SUN1 or SUN2 individually or in combination (Fig. 2). Western blot analysis confirmed efficient knockdown of SUN proteins under all conditions. Codepletion of SUN1 and SUN2 delayed NE/ER membrane removal similar to nocodazole treatment, whereas single knockdown of either SUN1 or SUN2 had no effect, indicating that both proteins share a redundant function in this process. The progression of NE/ER membrane removal in SUN1/2-codepleted cells was rescued upon expression of an RNAi-resistant SUN2-CFP construct (Figs. 2 and S1).

To test whether depletion of other INM proteins also influences NE/ER membrane retraction from chromatin, we depleted Lamin B receptor (LBR) or emerin. Knockdown of neither LBR nor emerin affected membrane remodeling (unpublished data), substantiating the idea that SUN proteins play a specific role in this process.

Down-regulation of the dynein regulators NudE/EL delays NE/ER membrane removal

Given that the dynein cofactors BICD2 and NudE/EL promote dynein association to the NE during mitotic entry (Hebbar et al., 2008; Splinter et al., 2010; Bolhy et al., 2011), we analyzed whether they play a role in removing NE/ER membranes from chromatin during prometaphase. Indeed, RNAi-mediated knockdown of NudE/EL perturbed membrane removal (Fig. 3). BICD2 depletion, in contrast, had no effect, suggesting that BICD2-dependent dynein recruitment to the NE is not involved in prometaphase NE/ER remodeling.

channel. To detect efflux of mPlum-GST-M9 into the cytoplasm, all images of the mPlum channel were processed in parallel by enhancing levels followed by setting γ correction to 0.5. (C) Removal of GFP-LAP2β–positive membranes from chromatin was determined using an ImageJ-based routine that measures the distance between the innermost NE/ER membrane and the outermost chromatin signal along 360 lines (blue lines; enlarged in boxed area) of a radial grid emanating from the center of mass of chromatin. (D) Reporter cells in early prophase were treated with DMSO or 333 nM nocodazole, cytochalasin D, or latrunculin B and imaged by confocal microscopy as described (A). Representative images show progression of membrane removal from chromatin at selected time points before and after NEBD. (E) Line blots show quantitative analysis comparing treatment with the different inhibitors (six experiments; means ± SEM; $n \geq 15$ per condition). Bars, 5 µm.

Published March 24, 2014

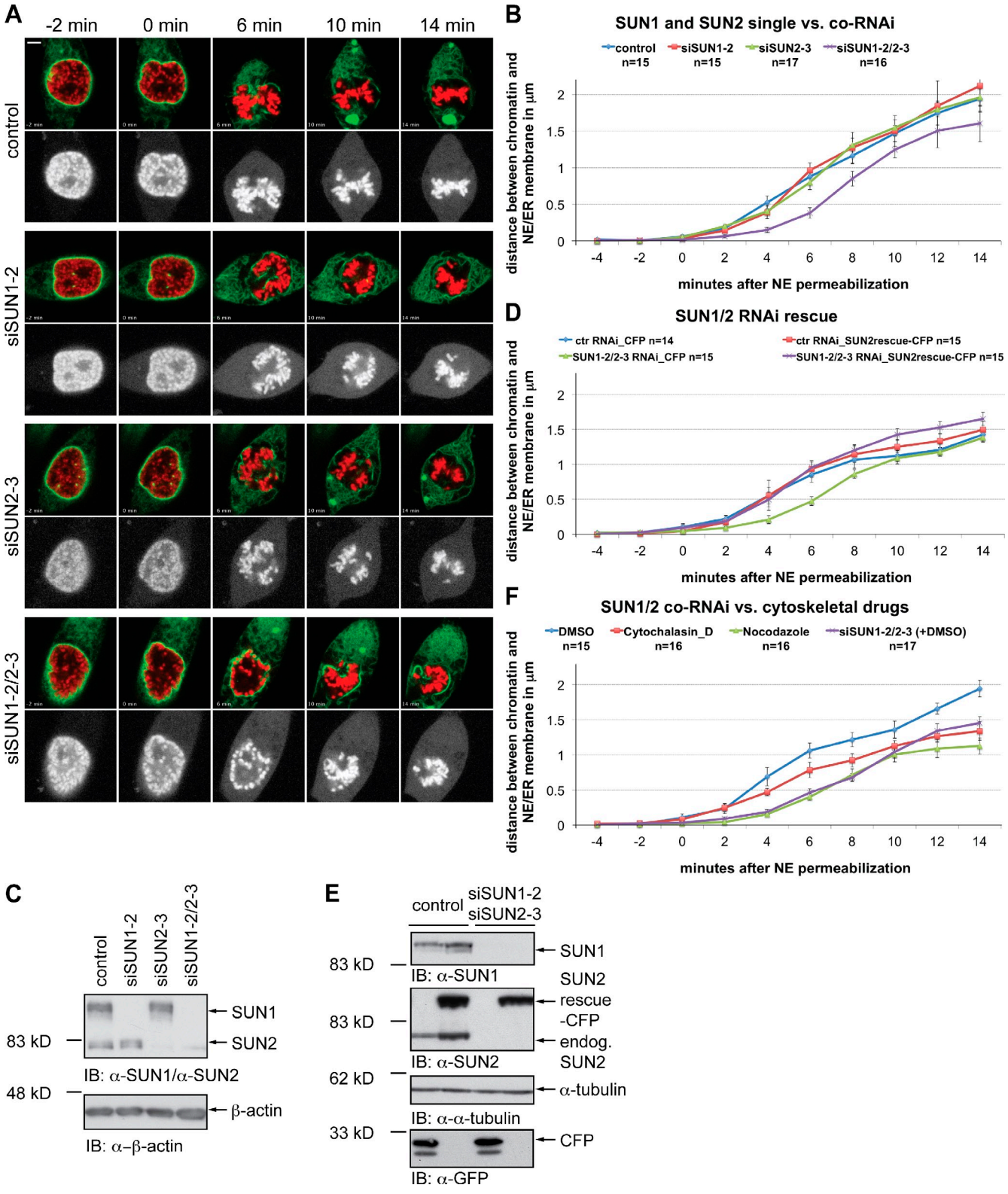

Figure 2. **SUN1/2 are functionally redundant in NE/ER membrane removal.** (A) Representative cells after control siRNA treatment or down-regulation of SUN1 and SUN2, either individually or combined, at the indicated time points before and after NEBD. Bar, 5 µm. (B, D, and F) Line blots displaying progression of NE/ER membrane removal from chromatin upon treatment with the indicated siRNAs or with 333 nM of the indicated cytoskeletal drugs (six and five experiments for B and D/F, respectively; means ± SEM; $n \geq 14$ per condition). (C and E) Western blots confirming efficient knockdown of SUN1/2 after 72 h of RNAi. β-Actin and α-tubulin serve as loading controls. ctr, control; endog., endogenous; IB, immunoblot.

Published March 24, 2014

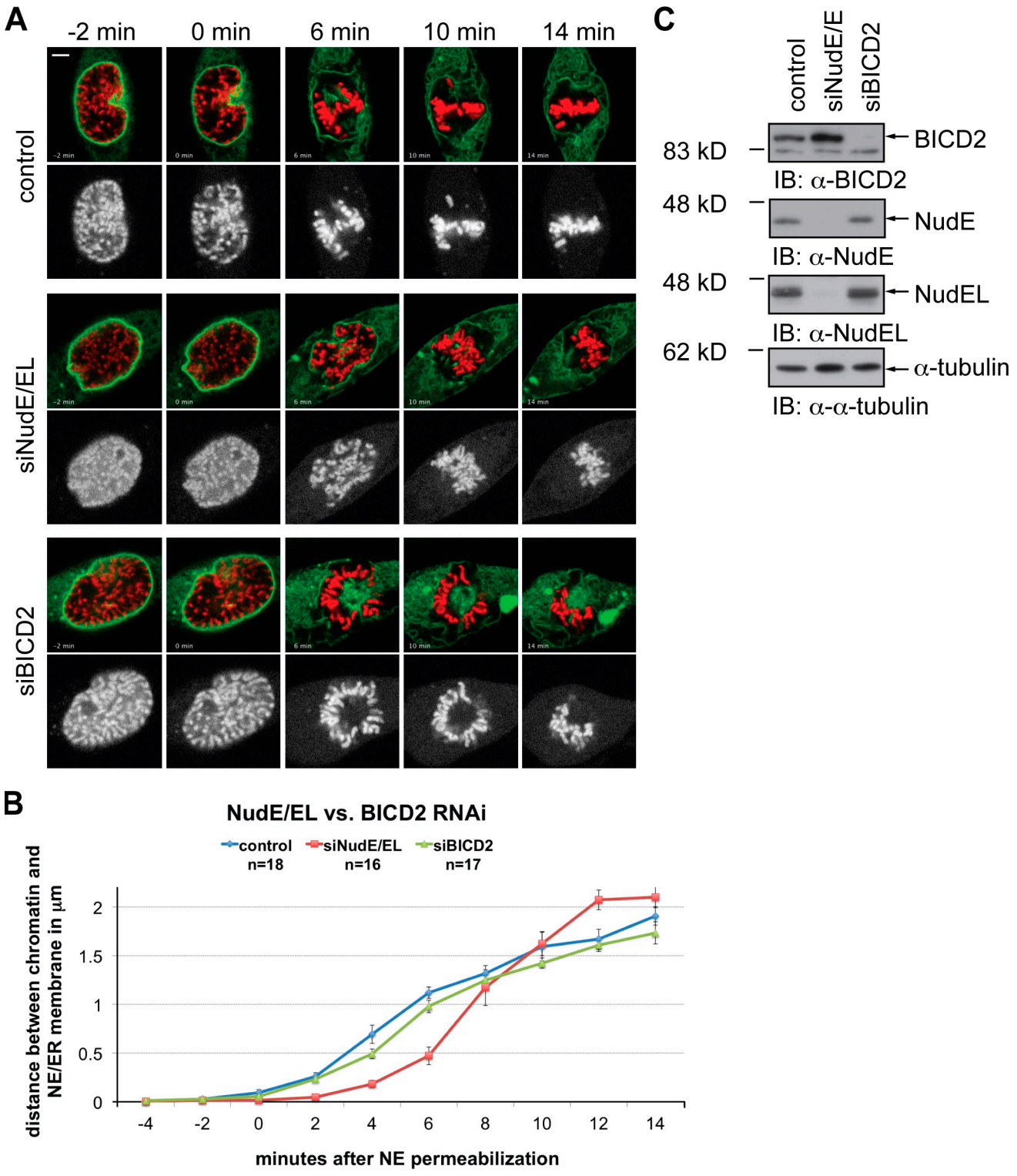

Figure 3. **Depletion of the dynein regulators NudE/EL delays NE/ER membrane removal from chromatin.** (A) Representative cells after depletion of NudE/EL or BICD2 at the indicated times before and after NEBD. Bar, 5 µm. (B) Line blot displaying the progression of NE/ER membrane removal from chromatin upon NudE/EL or BICD2 knockdown (five experiments; means ± SEM; $n \geq 16$ per condition). (C) Western blots to confirm efficient knockdown of the indicated proteins. α-Tubulin serves as loading control. IB, immunoblot.

Interestingly, the effect of NudE/EL RNAi resembled the one of SUN1/2 depletion, especially at early time points after the onset of NEBD, potentially indicating that dynein-driven NE/ER membrane remodeling relies on a mechanism involving both NudE/EL and SUN proteins. This notion is further supported by our observation that SUN1/2 codepletion impaired dynein recruitment to the NE in prophase cells similar to down-regulation of NudE/EL, indicating a connection between SUN proteins and

Published March 24, 2014

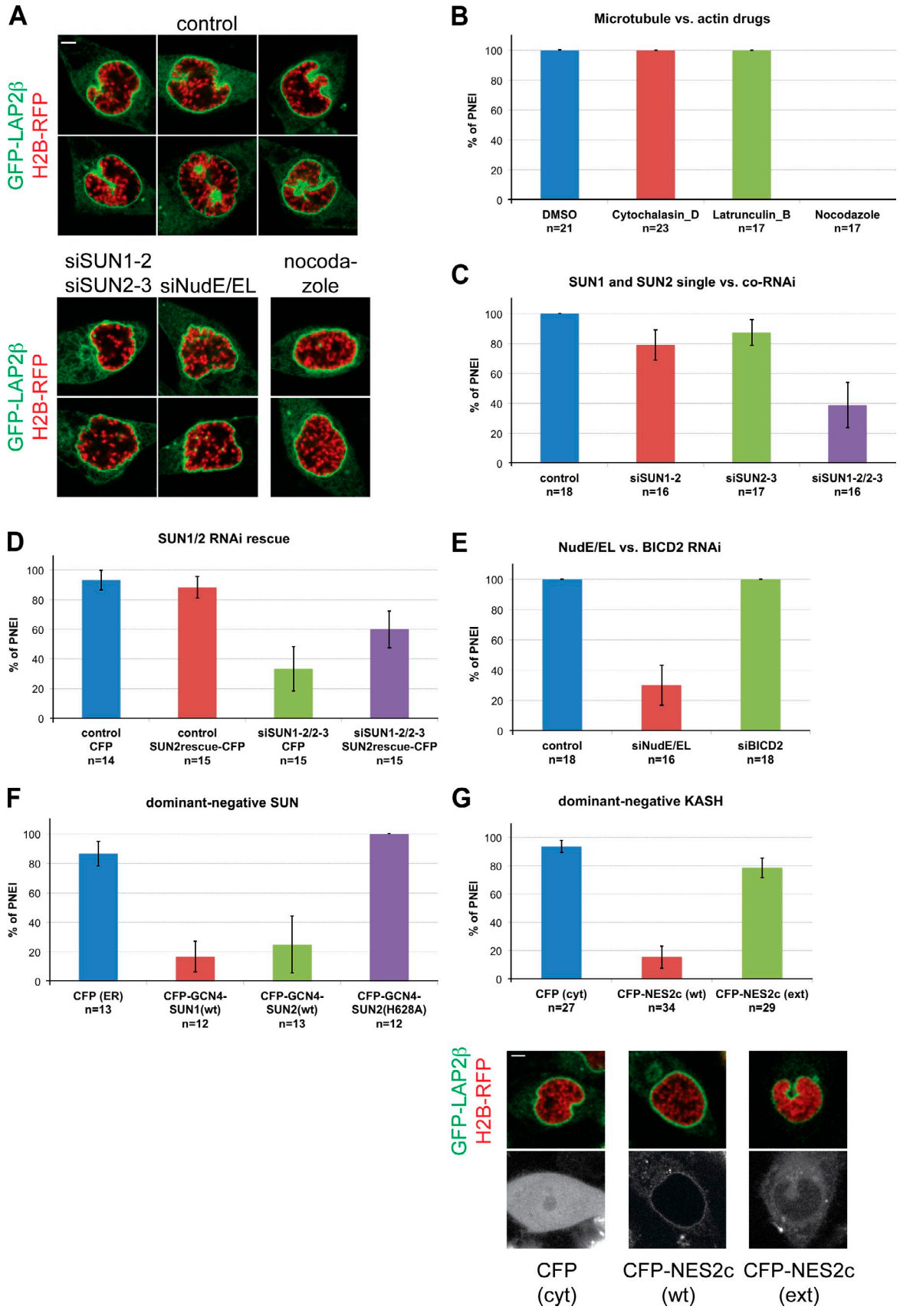

Figure 4. **LINC complexes contribute to the formation of PNEIs.** (A) Representative nuclei showing varying levels of PNEI observed upon the indicated treatments. (B–E) Nuclei of early prophase cells monitored by live-cell imaging were scored for PNEI. Nuclei were counted as PNEI positive if deep nuclear invaginations appeared before NEBD. Bar plots represent the percentage of nuclei with PNEI upon RNAi or the addition of cytoskeletal inhibitors (five

Published March 24, 2014

dynein (Fig. S2). Together, our results support a role of SUN1/2, NudE/EL, dynein, and MTs in the removal of NE/ER membranes from chromatin during NEBD.

LINC complex components contribute to the formation of PNEIs

NudE/EL have been described to contribute to the formation of PNEIs—NE pockets generated around centrosomes by NE-attached dynein (Hebbar et al., 2008; Bolhy et al., 2011). When we evaluated the occurrence of PNEI (Fig. 4), we found that nocodazole completely abolished PNEI as expected. Strikingly, codepletion of SUN1 and SUN2 also decreased the occurrence of PNEI to ∼35% of cells, whereas down-regulation of LBR or emerin had no effect (unpublished data). Overexpression of an RNAi-resistant SUN2-CFP fusion partially rescued the defect of SUN1/2 depletion and led to PNEI in ∼60% of cells. NudE/EL RNAi had a similar effect on PNEI as SUN1/2 depletion, whereas down-regulation of BICD2 showed no influence.

Previous experiments have revealed that loss of NudE/EL has a stronger impact on centrosome-NE tethering in prophase than depletion of CENP-F, indicating that NudE/EL might harbor an additional role outside the Nup133–CENP-F–NudE/EL axis (Bolhy et al., 2011). Interestingly, it has been noted that NudE/EL are homologues of *Caenorhabditis elegans* NUD2, a dynein regulator that interacts with the KASH protein UNC-83 to promote nuclear migration (Fridolfsson and Starr, 2010; Bolhy et al., 2011). Thus, NudE/EL, SUN1/2, and an ONM-resident KASH protein may constitute another protein complex supporting dynein-dependent NE remodeling during mitotic entry.

To test whether the function of SUN1 and SUN2 in PNEI formation might involve interactions with KASH proteins, we expressed dominant-negative (DN) SUN and KASH constructs (Fig. 4), which are known to interfere with the interaction of endogenous LINC constituents and cause a loss of Nesprins from the ONM (Crisp et al., 2006; Stewart-Hutchinson et al., 2008). The overexpression of soluble DN-SUN1 and DN-SUN2 in the ER lumen reduced PNEI formation to ∼20% of cells, whereas expression of an analogous SUN2 mutant (SUN2-H628A; Sosa et al., 2012) deficient in KASH binding had no effect. Similarly, we observed a strong reduction of PNEI upon expression of a DN-KASH protein but not of a mutant, C-terminally extended KASH construct that cannot displace Nesprins from the NE (Stewart-Hutchinson et al., 2008). These data indicate that the function of SUN proteins in prophase NE remodeling relies on their ability to cooperate with Nesprins in the ONM.

The SUN pathway emerges as a third mechanism for recruitment of dynein to the NE in prophase cells. Besides the two NPC-dependent pathways established by RanBP2–BICD2 and Nup133–CENP-F–NudE/EL (Splinter et al., 2010; Bolhy et al., 2011), LINC complexes could provide NE binding sites for dynein independent of nucleoporins. This might be especially important during early prometaphase when mitotic NPC disassembly has considerably advanced, as SUN and KASH proteins remain embedded in the ER membrane network throughout mitosis. We show that SUN protein depletion affects both PNEI and membrane removal from chromatin, indicating that SUN proteins promote NE/ER remodeling beyond NEBD. Currently, it is, however, unknown whether SUN and KASH proteins dissociate from each other during mitosis. Our results imply that LINC complexes may at least persist into early prometaphase.

Of the six vertebrate KASH proteins, only Nesprin-1, -2, and -3 are expressed in HeLa cells. Nesprin-1/2 are known to support dynein-dependent functions in interphase cells, including centrosome attachment to the nucleus in neural progenitor cells (Zhang et al., 2009), and are thus good candidates for a role in PNEI formation and perhaps NE/ER membrane removal from chromatin. It is, however, also conceivable that after NEBD, when INM proteins have been released into the ER, SUN proteins could act independently of KASH proteins by directly establishing a connection to dynein.

Codepletion of SUN1 and SUN2 affects mitotic spindle orientation, spindle structure, and centrosome integrity

To test whether depletion of SUN proteins affects later steps of mitosis, we first analyzed spindle morphology in fixed cells using α-tubulin and pericentrin antibodies (Fig. 5). Strikingly, many SUN1/2-depleted cells displayed spindles tilted relative to the division plane. Quantification of mitotic spindle orientation revealed an aberrant tilt of 30–90° in ∼30% of SUN1/2-codepleted cells, whereas <5% of control spindles fell into this range. Besides tilted spindles, we observed a large number of irregular mitotic spindles 72 h after SUN1/2 double knockdown.

To analyze spindle morphology in more detail, we used a HeLa cell line stably expressing centrin2-GFP and H2B-mCherry and determined the localization of pericentrin and α-tubulin by immunofluorescence. In control cells, mitotic spindles contained a regular number and morphology of poles. In contrast, in SUN1/2-codepleted cells, aberrant numbers of spindle poles were scored, frequently accompanied by fragmentation of pericentriolar material detected as ectopic clusters of pericentrin not associated with centrioles (Fig. 5). Under these conditions, chromatin was no longer organized in a compact metaphase plate. Quantification revealed an increase of disordered spindles in ∼45% of cells upon SUN1/2 codepletion compared with ∼3% of control cells. In contrast, the morphology and number of centrosomes in interphase cells codepleted of SUN1 and SUN2 remained unaffected (Fig. 5).

to six experiments; means ± SEM; $n \geq 14$ per condition). (F) PNEI analysis derived from videos of cells expressing CFP, CFP-GCN4-SUN1 (DN-SUN1), CFP-GCN4-SUN2 (DN-SUN2), or CFP-GCN4-SUN2(H628A) in the lumen of the ER 48 h after transfection (five experiments; means ± SEM; $n \geq 12$ per condition). (G) PNEI analysis derived from videos of reporter cells expressing cytoplasmic (cyt) CFP, CFP-NES2c (wild type [wt]; DN-KASH2), or C-terminally extended (ext) CFP-NES2c 48 h after transfection (seven experiments; means ± SEM; $n \geq 27$ per condition). (bottom) CFP fluorescence of the respective proteins is shown. Bars, 5 µm.

Published March 24, 2014

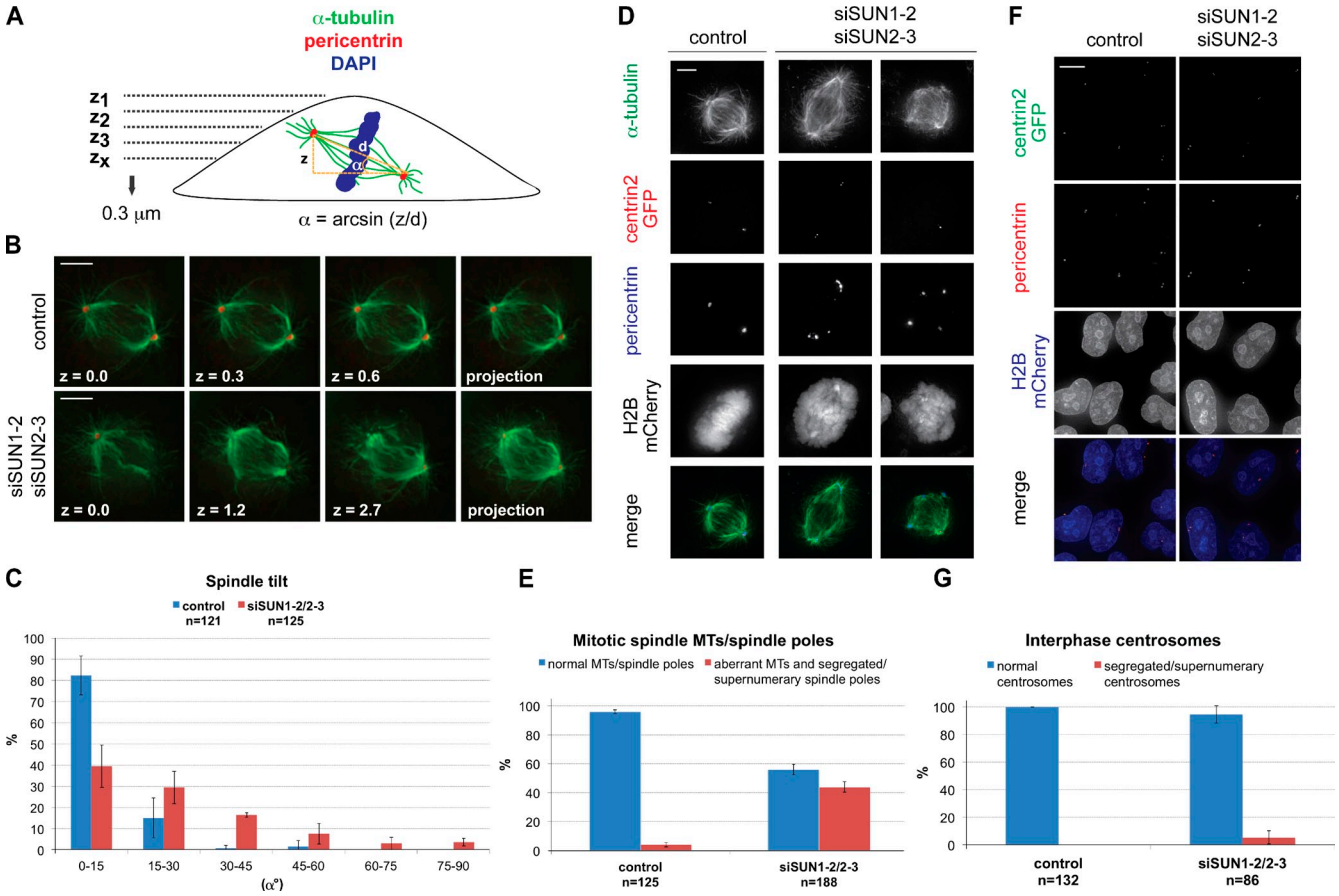

Figure 5. **Loss of SUN1/2 results in changes of spindle tilt and morphology.** (A) Schematic representation of the experimental approach to determine spindle pole-to-pole distance and tilt. Stacks of 0.3-µm sections were analyzed. Spindle length (d) was measured as the distance of the centrosomes in 3D. Spindle tilt is represented by the angle α, which is calculated as the arcsin of the pole-to-pole distance in z divided by d. (B) Immunofluorescence of spindles in control RNAi or SUN1/2-depleted cells using α-tubulin and pericentrin antibodies. Representative images are shown as three scans of different z sections and their maximum intensity projections. (C) Quantitative analysis of tilted spindles displayed by the distribution of cells into classes of spindle angles (α in degrees) from $n \geq 121$ (three experiments; means ± SD). (D) HeLa cells stably expressing H2B-mCherry and centrin2-GFP were depleted of SUN1/2 by RNAi for 72 h. Images show mitotic cells stained for α-tubulin and pericentrin. (E) Bar plot representing the mean percentage of defective spindles (aberrant MTs and segregated/supernumerary spindle poles) upon SUN1/2 RNAi compared with control cells (three experiments; means ± SD; $n \geq 40$ per condition and experiment). (F) Cells as in D were stained for pericentrin. (G) Bar plot representing the mean percentage of segregated/supernumerary interphase centrosomes upon SUN1/2 RNAi compared with control cells (three experiments; $n \geq 86$ per condition; means ± SD). Bars: (B and D) 5 µm; (F) 10 µm.

Codepletion of SUN1 and SUN2 affects mitotic progression

When we scored cell numbers at different time points after SUN1/2 RNAi, we observed that the number of SUN1/2-codepleted cells dropped to ∼75% after 72 h and ∼60% after 96 h of RNAi compared with control cells (Fig. S3). To elucidate whether perturbed mitotic progression might contribute to slowed cell proliferation, we used live-cell imaging of a HeLa cell line expressing an importin-β binding (IBB) fusion with GFP (IBB-GFP) as the NE disassembly/reassembly marker and H2B-mCherry as a chromatin marker (Held et al., 2010). The time spans from nuclear efflux of IBB-GFP at NEBD to chromatin separation and from anaphase onset to nuclear accumulation of IBB-GFP were determined using CellCognition (Held et al., 2010). Although control cells initiated chromatin separation on average within 35–40 min after NEBD, SUN1/2-depleted cells showed a delay of ∼20 min (Fig. S3). Many cells depleted for SUN1/2 displayed perturbations in formation, stability, and alignment of the metaphase plate, supporting our results on spindle orientation in fixed cells (Fig. 5). Spindle formation in SUN1/2-codepleted cells was often accompanied by spindle tumbling (Videos 1 and 2). These cells then finally initiated chromatin segregation, often with not properly aligned spindles, or went into apoptosis. The timing between anaphase onset and IBB-GFP import was only slightly affected by SUN1/2 depletion.

The spindle defects, i.e., in spindle morphology and stability, are probably not a direct consequence of preceding delays in NE/ER remodeling but could reflect a separate function of SUN proteins affecting mitosis. As SUN proteins have been implicated in centrosome duplication (Starr and Fridolfsson, 2010), one possibility is that spindle defects arise from failures in centrosome duplication and/or maturation in interphase. Analysis of interphase cells, however, showed no apparent changes in centrosome number and morphology upon SUN1/2 depletion (Fig. 5); yet, centrosome defects may only materialize by disintegration of spindle poles in mitosis. It is thus also worth considering that mitotic centrosome aberrations could contribute to the reduction of PNEI and delays in NE removal from chromatin.

Published March 24, 2014

Defects in spindle assembly accompanied by spindle pole fragmentation have been observed before, for example, upon depletion of TOGp, cytoplasmic linker-associated protein (Cassimeris and Morabito, 2004; Logarinho et al., 2012), Aurora A (Asteriti et al., 2011), and IFT88 (Delaval et al., 2011), and explained by an imbalance of forces exerted by motor proteins required for maintenance of spindle pole integrity. As the spindle tumbling phenotype upon SUN protein depletion often developed readily after mitotic entry, it is, in analogy, also conceivable that SUN proteins influence motor proteins, such as dynein, involved in establishing the balance of forces within the spindle.

A speculative scenario invoking a more direct role of SUN proteins in the maintenance of a stable spindle is their contribution as constituents of the mitotic ER, which surrounds the spindle occupying most of the cytoplasm. This membranous spindle cocoon could facilitate spindle stability either directly by providing subcortical binding sites for astral MTs or more indirectly by organizing the bulk cytoplasmic actomyosin network. Actomyosin is important for spindle assembly and positioning (Rosenblatt, 2005). A model taking into account our observations would entail a cross talk between the ER and the actin cytoskeleton mediated by LINC complex components distributed through the mitotic membrane network of the ER. A stabilizing membrane-associated subcortex could explain how membrane proteins with well-established functions in interphase could influence not only NEBD but also spindle formation and mitotic progression, important events implicated in the development of severe diseases such as cancer.

Materials and methods

Molecular cloning

The coding sequence of LAP2β (aa 244–453) was inserted into the HindIII and BamHI sites of pEGFP-C3 (Takara Bio Inc.) and has been described previously (Mühlhäusser and Kutay, 2007). Full-length H2B-mRFP was expressed from a pIRESpuro2 vector (Takara Bio Inc.) as described previously (Mühlhäusser and Kutay, 2007). The pIRES mPlum-GST-M9 vector was generated and provided by A. Rothballer (Institute of Biochemistry, Swiss Federal Institute of Technology Zurich, Zurich, Switzerland) by first replacing the coding sequence of EGFP in pEGFP-C1 (Takara Bio Inc.) by the coding sequence of mPlum and then inserting the coding sequence of the GST-M9 fusion protein (Mühlhäusser and Kutay, 2007) into the BglII and HindIII sites. Afterward, the coding sequence of mPlum-GST-M9 was subcloned into the Nhe–BamHI of pIREShygro (Takara Bio Inc.). The coding sequence of centrin2-GFP was subcloned into the EcoRI–NotI sites of pIRES-puro2 (Takara Bio Inc.). The RNAi-resistant full-length SUN2 coding sequence was purchased from GeneArt (Life Technologies) and cloned into the BglII–EcoRI sites of pECFP-N3 (Takara Bio Inc.).

For the generation of DN-SUN1 and DN-SUN2, the SUN domain of either SUN1 or SUN2 was appended to an ER signal sequence followed by CFP and a trimerizing coiled-coil derived from yeast GCN4 (Ciani et al., 2010), which allows the SUN fragments to adopt a KASH-binding competent trimeric organization (Sosa et al., 2012). In pCMV/myc/ER/GFP (Invitrogen), the coding sequence of GFP was replaced for that of ECFP, inserted into the PstI–NotI sites. For further cloning, a SalI site was introduced upstream of NotI. SUN1(724–916), SUN2(507–717), and SUN2(507–717)H628A, N-terminally fused to a trimerizing variant of the coiled-coil region of GCN4, were subcloned into the SalI–NotI site of pCMV/myc/ER/ECFP. GCN4-SUN2(507–717) and the dysfunction of SUN2(H628A) in KASH binding have been described previously (Sosa et al., 2012). DN-KASH2 was generated by inserting the C-terminal domain of Nesprin-2 (corresponding to the last 331 aa) into the XhoI–BamHI site of pECFP-C1 (Takara Bio Inc.). KASH2(extension) was derived from the DN-KASH2 construct by adding a C-terminal extension of 13 aa (VDGTAGPGSTGSR; Stewart-Hutchinson et al., 2008). Expression of all constructs was under control of a cytomegalovirus promoter.

Cell lines, cell culture, and transient transfection

mPlum-GST-M9 was introduced into a HeLa cell line stably expressing GFP-LAP2β and H2B-mRFP (Mühlhäusser and Kutay, 2007) followed by selection for positive clones with 300 µg/ml hygromycin. Triple stable clones were selected with 500 µg/ml G418, 0.5 µg/ml puromycin, and 300 µg/ml hygromycin. Centrin2-GFP was introduced into a HeLa cell line stably expressing H2B-mCherry followed by selection for positive clones with 0.5 µg/ml puromycin. Double stable clones were selected with 500 µg/ml G418 and 0.5 µg/ml puromycin. For RNAi rescue experiments, HeLa cells were electroporated with a construct expressing an RNAi-resistant SUN2-CFP fusion using the nucleofection kit (Nucleofector; Amaxa).

HeLa cells were maintained in DMEM (Sigma-Aldrich) containing 10% FCS (PAA Laboratories) and 100 µg/ml penicillin/streptomycin (PAA Laboratories) and appropriate selection drugs at 37°C and 5% CO_2 in a humidified incubator. For in vivo imaging, cells were cultured in chambered coverglasses (Lab-Tek II; Thermo Fisher Scientific) in complete DMEM without phenol red and riboflavin (Invitrogen) containing 10% FCS and 100 µg/ml penicillin/streptomycin. Transient transfections were performed using transfection reagent (X-tremeGENE 9; Roche) according to the manufacturer's protocol.

RNAi

RNAi was performed using transfection reagent (INTERFERin; Polyplus) according to the manufacturer's protocol. siRNAs were purchased from QIAGEN or Microsynth. For siRNA transfection, HeLa cells were grown to a confluency of 50–60% in 6-well dishes, and transfection was performed at a final siRNA concentration of 10 nM per target gene. Before transfection, cells were transferred to fresh DMEM (Sigma-Aldrich). 48–96 h after transfection, cells were either fixed for immunofluorescence analysis or harvested for Western blot analysis. For live-cell imaging, cells were reseeded on chambered coverglasses (Lab-Tek II) 48 h after siRNA transfection. Microscopy was performed after 72 h of RNAi treatment. For rescue experiments, HeLa cells were electroporated with RNAi-resistant SUN2-CFP before replating for 3 h and RNAi treatment. Rescue analysis was performed 72 h after siRNAi transfection. The following siRNAs were used in this study: AllStars (siRNA control) siSUN1-2 (5′-TTACCAGGTGCCTTCGAAA-3′), siSUN2-3 (5′-TGGCAGAGATGCAGGGCAA-3′), and siBICD2#2, (Splinter et al., 2010; Bolhy et al., 2011); siNudE/EL mix siNudE (5′-GGACCCAGCTCAAGTTTAATT-3′ and 5′-GGAAAGATCTGGCGATGACTT-3′) and siNudEL (5′-GCTAGGATATCAGCACTAATT-3′ and 5′-GGACCAAGCATCACGAAAATT-3′; Vergnolle and Taylor, 2007; Bolhy et al., 2011); and siPLK (5′-CGCGGGCAAGATTGTGCCTAA-3′).

Counting cells

To determine the cell number after RNAi treatment, cells were washed with PBS and detached from cell culture dishes using 0.5 mM EDTA in PBS. Next, cells were automatically counted using a Cellometer Auto T4 (Nexcelom), pelleted with 2,000 rpm for 5 min at 4°C, and resuspended in SDS sample buffer. Subsequently, cell lysates were subjected to SDS-PAGE and Western blot analysis to determine RNAi knockdown efficiency.

Antibodies

Rabbit polyclonal antibodies to human SUN1 and SUN2 have been previously described (Turgay et al., 2010; Sosa et al., 2012). Antibodies against GFP and human full-length NudE were generated in rabbits and affinity purified. The mouse monoclonal antibodies against α-tubulin (T5168) and β-actin (A1978) were purchased from Sigma-Aldrich. The rabbit polyclonal antibodies against BICD2 (ab73286), pericentrin (ab4448), and NudEL (ab25959) were purchased from Abcam. Rabbit polyclonal anti–β-actin (A2066) was obtained from Sigma-Aldrich, and mouse monoclonal anti–dynein intermediate chain (DIC; ab23905) was obtained from Abcam.

Inhibitors

Nocodazole, cytochalasin D, and latrunculin B were purchased from Sigma-Aldrich. These drugs were used at levels that efficiently interfered with the dynamic properties of the cytoskeleton but did not induce vast morphological changes of cell shape.

Immunofluorescence analysis

For investigation of the spindle/interphase centrosome morphology, cells were treated with cold cytoskeleton buffer (60 mM Pipes, pH 6.8, 25 mM Hepes, pH 7.4, 10 mM EGTA, pH 8, 4 mM $MgSO_4$, and 0.5% Triton X-100) containing 5 µM taxol for 1 min before fixation in ice-cold methanol or 4% PFA for 5 or 10 min, respectively. Immunostaining was performed using anti–α-tubulin and anti-pericentrin antibodies. After washing with PBS,

Published March 24, 2014

coverslips were mounted in Vectashield (Vector Laboratories) for microscopic analysis.

For the analysis of dynein recruitment to the NE during G2/M, siRNA-treated cells were subjected to 10 µM nocodazole for 5 h as described previously (Splinter et al., 2010). Before immunostaining with anti-DIC, cells were fixed with ice-cold methanol for 10 min. DNA was stained with DAPI, and samples were prepared for confocal microscopy. The NE/ER ratio of the DIC immunofluorescence signal was calculated using MatLAB. In brief, the mean fluorescence intensity within a 5-pixel-wide circle enclosing the NE (nuclear boundary defined by the outermost border of DAPI fluorescence, reaching to 2 pixels into the nucleus and 3 pixels into the cytoplasm) was divided by the mean fluorescence intensity within a 15-pixel-wide ring adjacent to the NE circle.

Widefield microscopy

Widefield microscopy of fixed samples was performed at room temperature on a DeltaVision Microscope (IX-71; Olympus) connected to a camera (CoolSNAP HQ; Photometrics), using a differential interference contrast Plan Apochromat 100×, NA 1.4 oil immersion objective. Fluorescent dyes (DAPI, Alexa Fluor 488, Alexa Fluor 633, GFP, and mCherry) were excited using a mercury short arc lamp and the corresponding filter settings. To visualize the complete volume of a mitotic spindle, stacks of 0.3-µm slices were acquired. Images of all channels were deconvolved using three iterations in softWoRx (Applied Precision).

Confocal microscopy

Live-cell imaging was performed using a 63×, NA 1.4 differential interference contrast Plan Apochromat oil immersion objective (Carl Zeiss) mounted on a customized confocal microscope (excitation 405, 488, and 561 nm for CFP, GFP, and RFP, respectively; LSM 710; Carl Zeiss) equipped with a temperature- and CO_2-controlled incubator box (37°C and 5% CO_2). To monitor NEBD and for subsequent measurements of distances between chromatin and NE/ER membranes, stacks of 512 × 512 × 4 µm with a width of 33.74 µm (resulting in a pixel width of 65.9 nm) and a step size of 1 µm were acquired every 2 min (pixel dwell time of 1.27 µs; line average of 8) using low laser intensities to reduce phototoxicity. Live-cell imaging was performed in DMEM containing 10% (vol/vol) FCS and 1% (vol/vol) penicillin–streptomycin but without phenol red and riboflavin to reduce autofluorescence of the medium.

Live-cell imaging (mitotic progression)

Mitotic progression was analyzed using a HeLa cell line stably expressing IBB-GFP and H2B-mCherry or GFP–α-tubulin and H2B-mCherry (Held et al., 2010). Live-cell imaging in a screening format (96-well; Greiner Bio One) was performed with a microscope (ImageXpress; Molecular Devices) connected to a camera (CoolSNAP HQ), using an S Fluor 10×, NA 0.5 air objective. Experiments were performed in a humidified incubator at 37°C and 5% CO_2 using DMEM containing 10% (vol/vol) FCS and 1% (vol/vol) penicillin–streptomycin but without phenol red and riboflavin to reduce autofluorescence of the medium. Fluorescent dyes were illuminated with a xenon lamp (IBB-GFP/H2B-mCherry) or light-emitting diode lamp (GFP–α-tubulin/H2B-mCherry) at low light intensity. To ensure treatment with the same light intensity throughout independent experiments, the Xenon lamp was calibrated before imaging. Usage of a 10× objective allowed imaging of only one slice per channel to follow mitotic cells and reduced phototoxicity. Images were acquired with a time interval of 3.5 min (IBB-GFP/H2B-mCherry) or 2.5 min (GFP–α-tubulin/H2B-mCherry). Mitotic timing was determined using the CeCogAnalyzer 1.0.7.0 (Held et al., 2010).

Image analysis and quantification

Images were further analyzed and processed using ZEN 2010 (Carl Zeiss) and ImageJ (National Institutes of Health). Image analysis of confocal live-cell experiments on NE/ER membrane tearing relied on an automated ImageJ-based measuring routine to determine the distance between NE/ER membranes and chromatin at different time points of NEBD. After adaptive thresholding and despeckling of all images, the convex hull algorithm was applied on the green LAP2β channel to define the outermost contours of NE/ER membranes. The ABSnake algorithm was applied on the red H2B channel using 10 iterations to delineate the outermost contours of chromatin. The distance between the innermost NE/ER membrane and the outermost chromatin signal was measured along 360 lines of a radial grid emanating from the center of mass of the chromatin structure. Sampled data containing all distance information from four z slices per time point were processed using Excel (Microsoft). Note that to detect efflux of mPlum-GST-M9 into the cytoplasm, all images of the mPlum channel were processed in parallel by enhancing levels followed by setting γ correction to 0.5.

Online supplemental material

Fig. S1 demonstrates that expression of an RNAi-resistant SUN2 construct rescues the delay in NE/ER membrane removal otherwise induced by SUN1/2 knockdown. Fig. S2 provides evidence that the recruitment of dynein to the NE is reduced upon SUN1/2 depletion. In Fig. S3, it is shown that down-regulation of SUN1/2 affects cell proliferation and prolongs mitosis. Videos 1 and 2 show HeLa cells expressing H2B-mCherry and GFP–α-tubulin treated with control and SUN1-2/2-3 siRNAs, respectively, and document spindle tumbling in SUN1/2-depleted cells. A text file is also provided that shows an ImageJ plugin for distance measurements between chromatin and NE/ER membranes along the lines of a radial grid. Online supplemental material is available at http://www.jcb.org/cgi/content/full/jcb.201310116/DC1. Additional data are available in the JCB DataViewer at http://dx.doi.org/10.1083/jcb.201310116.dv.

We thank A. Rothballer for reagents, P. Horvath for help with image analysis, A. Rothballer and C. Wandke for critical reading, and G. Csucs, J. Hehl, and J. Kusch of the Light Microscopy and Screening Center for support.

This work was funded by a Boehringer Ingelheim fellowship and an UBS Promedica grant to Y. Turgay and by grants of the Swiss National Science Foundation (310030-313135) and European Research Council (NucEnv) to U. Kutay.

The authors declare no competing financial interests.

Author contributions: U. Kutay defined the research theme. U. Kutay and Y. Turgay conceptualized the strategy, methods, and experiments. Y. Turgay performed and analyzed most experiments, except for Fig. S2, parts of Fig. 4, and Videos 1 and 2 (by L. Champion). C. Balazs created the ImageJ-based image analysis tool. M. Held and D.W. Gerlich assisted in data analysis for Fig. S3. A. Toso and P. Meraldi helped with initial analysis of the spindle tilt. P. Meraldi gave advice throughout the study. U. Kutay and Y. Turgay discussed analyses, interpretations, and presentation and wrote the manuscript.

Submitted: 25 October 2013
Accepted: 26 February 2014

References

Asteriti, I.A., M. Giubettini, P. Lavia, and G. Guarguaglini. 2011. Aurora-A inactivation causes mitotic spindle pole fragmentation by unbalancing microtubule-generated forces. *Mol. Cancer*. 10:131. http://dx.doi.org/10.1186/1476-4598-10-131

Beaudouin, J., D. Gerlich, N. Daigle, R. Eils, and J. Ellenberg. 2002. Nuclear envelope breakdown proceeds by microtubule-induced tearing of the lamina. *Cell*. 108:83–96. http://dx.doi.org/10.1016/S0092-8674(01)00627-4

Bolhy, S., I. Bouhlel, E. Dultz, T. Nayak, M. Zuccolo, X. Gatti, R. Vallee, J. Ellenberg, and V. Doye. 2011. A Nup133-dependent NPC-anchored network tethers centrosomes to the nuclear envelope in prophase. *J. Cell Biol.* 192:855–871. http://dx.doi.org/10.1083/jcb.201007118

Cassimeris, L., and J. Morabito. 2004. TOGp, the human homolog of XMAP215/Dis1, is required for centrosome integrity, spindle pole organization, and bipolar spindle assembly. *Mol. Biol. Cell*. 15:1580–1590. http://dx.doi.org/10.1091/mbc.E03-07-0544

Chikashige, Y., C. Tsutsumi, M. Yamane, K. Okamasa, T. Haraguchi, and Y. Hiraoka. 2006. Meiotic proteins bqt1 and bqt2 tether telomeres to form the bouquet arrangement of chromosomes. *Cell*. 125:59–69. http://dx.doi.org/10.1016/j.cell.2006.01.048

Ciani, B., S. Bjelic, S. Honnappa, H. Jawhari, R. Jaussi, A. Payapilly, T. Jowitt, M.O. Steinmetz, and R.A. Kammerer. 2010. Molecular basis of coiled-coil oligomerization-state specificity. *Proc. Natl. Acad. Sci. USA*. 107:19850–19855. http://dx.doi.org/10.1073/pnas.1008502107

Crisp, M., Q. Liu, K. Roux, J.B. Rattner, C. Shanahan, B. Burke, P.D. Stahl, and D. Hodzic. 2006. Coupling of the nucleus and cytoplasm: role of the LINC complex. *J. Cell Biol.* 172:41–53. http://dx.doi.org/10.1083/jcb.200509124

Delaval, B., A. Bright, N.D. Lawson, and S. Doxsey. 2011. The cilia protein IFT88 is required for spindle orientation in mitosis. *Nat. Cell Biol.* 13:461–468. http://dx.doi.org/10.1038/ncb2202

Fridolfsson, H.N., and D.A. Starr. 2010. Kinesin-1 and dynein at the nuclear envelope mediate the bidirectional migrations of nuclei. *J. Cell Biol.* 191:115–128. http://dx.doi.org/10.1083/jcb.201004118

Fridolfsson, H.N., N. Ly, M. Meyerzon, and D.A. Starr. 2010. UNC-83 coordinates kinesin-1 and dynein activities at the nuclear envelope during nuclear migration. *Dev. Biol.* 338:237–250. http://dx.doi.org/10.1016/j.ydbio.2009.12.004

Güttinger, S., E. Laurell, and U. Kutay. 2009. Orchestrating nuclear envelope disassembly and reassembly during mitosis. *Nat. Rev. Mol. Cell Biol.* 10:178–191. http://dx.doi.org/10.1038/nrm2641

Hebbar, S., M.T. Mesngon, A.M. Guillotte, B. Desai, R. Ayala, and D.S. Smith. 2008. Lis1 and Ndel1 influence the timing of nuclear envelope breakdown in neural stem cells. *J. Cell Biol.* 182:1063–1071. http://dx.doi.org/10.1083/jcb.200803071

Held, M., M.H.A. Schmitz, B. Fischer, T. Walter, B. Neumann, M.H. Olma, M. Peter, J. Ellenberg, and D.W. Gerlich. 2010. CellCognition: time-resolved phenotype annotation in high-throughput live cell imaging. *Nat. Methods*. 7:747–754. http://dx.doi.org/10.1038/nmeth.1486

Logarinho, E., S. Maffini, M. Barisic, A. Marques, A. Toso, P. Meraldi, and H. Maiato. 2012. CLASPs prevent irreversible multipolarity by ensuring spindle-pole resistance to traction forces during chromosome alignment. *Nat. Cell Biol.* 14:295–303. http://dx.doi.org/10.1038/ncb2423

Malone, C.J., W.D. Fixsen, H.R. Horvitz, and M. Han. 1999. UNC-84 localizes to the nuclear envelope and is required for nuclear migration and anchoring during *C. elegans* development. *Development*. 126:3171–3181.

Malone, C.J., L. Misner, N. Le Bot, M.-C. Tsai, J.M. Campbell, J. Ahringer, and J.G. White. 2003. The *C. elegans* hook protein, ZYG-12, mediates the essential attachment between the centrosome and nucleus. *Cell*. 115:825–836. http://dx.doi.org/10.1016/S0092-8674(03)00985-1

Morimoto, A., H. Shibuya, X. Zhu, J. Kim, K.-I. Ishiguro, M. Han, and Y. Watanabe. 2012. A conserved KASH domain protein associates with telomeres, SUN1, and dynactin during mammalian meiosis. *J. Cell Biol.* 198:165–172. http://dx.doi.org/10.1083/jcb.201204085

Mühlhäusser, P., and U. Kutay. 2007. An in vitro nuclear disassembly system reveals a role for the RanGTPase system and microtubule-dependent steps in nuclear envelope breakdown. *J. Cell Biol.* 178:595–610. http://dx.doi.org/10.1083/jcb.200703002

Raaijmakers, J.A., R.G. van Heesbeen, J.L. Meaders, E.F. Geers, B. Fernandez-Garcia, R.H. Medema, and M.E. Tanenbaum. 2012. Nuclear envelope-associated dynein drives prophase centrosome separation and enables Eg5-independent bipolar spindle formation. *EMBO J.* 31:4179–4190. http://dx.doi.org/10.1038/emboj.2012.272

Rosenblatt, J. 2005. Spindle assembly: asters part their separate ways. *Nat. Cell Biol.* 7:219–222. http://dx.doi.org/10.1038/ncb0305-219

Salina, D., K. Bodoor, D.M. Eckley, T.A. Schroer, J.B. Rattner, and B. Burke. 2002. Cytoplasmic dynein as a facilitator of nuclear envelope breakdown. *Cell*. 108:97–107. http://dx.doi.org/10.1016/S0092-8674(01)00628-6

Schlaitz, A.L., J. Thompson, C.C. Wong, J.R. Yates III, and R. Heald. 2013. REEP3/4 ensure endoplasmic reticulum clearance from metaphase chromatin and proper nuclear envelope architecture. *Dev. Cell*. 26:315–323. http://dx.doi.org/10.1016/j.devcel.2013.06.016

Sosa, B.A., A. Rothballer, U. Kutay, and T.U. Schwartz. 2012. LINC complexes form by binding of three KASH peptides to domain interfaces of trimeric SUN proteins. *Cell*. 149:1035–1047. http://dx.doi.org/10.1016/j.cell.2012.03.046

Splinter, D., M.E. Tanenbaum, A. Lindqvist, D. Jaarsma, A. Flotho, K.L. Yu, I. Grigoriev, D. Engelsma, E.D. Haasdijk, N. Keijzer, et al. 2010. Bicaudal D2, dynein, and kinesin-1 associate with nuclear pore complexes and regulate centrosome and nuclear positioning during mitotic entry. *PLoS Biol.* 8:e1000350. http://dx.doi.org/10.1371/journal.pbio.1000350

Starr, D.A., and H.N. Fridolfsson. 2010. Interactions between nuclei and the cytoskeleton are mediated by SUN-KASH nuclear-envelope bridges. *Annu. Rev. Cell Dev. Biol.* 26:421–444. http://dx.doi.org/10.1146/annurev-cellbio-100109-104037

Starr, D.A., and M. Han. 2002. Role of ANC-1 in tethering nuclei to the actin cytoskeleton. *Science*. 298:406–409. http://dx.doi.org/10.1126/science.1075119

Stewart-Hutchinson, P.J., C.M. Hale, D. Wirtz, and D. Hodzic. 2008. Structural requirements for the assembly of LINC complexes and their function in cellular mechanical stiffness. *Exp. Cell Res.* 314:1892–1905. http://dx.doi.org/10.1016/j.yexcr.2008.02.022

Turgay, Y., R. Ungricht, A. Rothballer, A. Kiss, G. Csucs, P. Horvath, and U. Kutay. 2010. A classical NLS and the SUN domain contribute to the targeting of SUN2 to the inner nuclear membrane. *EMBO J.* 29:2262–2275. http://dx.doi.org/10.1038/emboj.2010.119

Vergnolle, M.A., and S.S. Taylor. 2007. Cenp-F links kinetochores to Ndel1/Nde1/Lis1/dynein microtubule motor complexes. *Curr. Biol.* 17:1173–1179. http://dx.doi.org/10.1016/j.cub.2007.05.077

Worman, H.J., and G.G. Gundersen. 2006. Here come the SUNs: a nucleocytoskeletal missing link. *Trends Cell Biol.* 16:67–69. http://dx.doi.org/10.1016/j.tcb.2005.12.006

Wynne, D.J., O. Rog, P.M. Carlton, and A.F. Dernburg. 2012. Dynein-dependent processive chromosome motions promote homologous pairing in *C. elegans* meiosis. *J. Cell Biol.* 196:47–64. http://dx.doi.org/10.1083/jcb.201106022

Yu, J., K. Lei, M. Zhou, C.M. Craft, G. Xu, T. Xu, Y. Zhuang, R. Xu, and M. Han. 2011. KASH protein Syne-2/Nesprin-2 and SUN proteins SUN1/2 mediate nuclear migration during mammalian retinal development. *Hum. Mol. Genet.* 20:1061–1073. http://dx.doi.org/10.1093/hmg/ddq549

Zhang, X., K. Lei, X. Yuan, X. Wu, Y. Zhuang, T. Xu, R. Xu, and M. Han. 2009. SUN1/2 and Syne/Nesprin-1/2 complexes connect centrosome to the nucleus during neurogenesis and neuronal migration in mice. *Neuron*. 64:173–187. http://dx.doi.org/10.1016/j.neuron.2009.08.018